University of Massachusetts Amherst

From the SelectedWorks of Panos Kevrekidis

October 23, 2012

Nonlinear PT-symmetric plaquettes

Kai Li, *University of Massachusetts - Amherst*
Panos Kevrekidis
Boris A. Malomed
Uwe Günther

Available at: https://works.bepress.com/panos_kevrekidis/210/

Nonlinear $\mathcal{PT}-$symmetric plaquettes

Kai Li and P. G. Kevrekidis
Department of of Mathematics and Statistics,
University of Massachusetts,
Amherst, MA 01003-9305, USA

Boris A. Malomed
Department of Physical Electronics,
School of Electrical Engineering, Faculty of Engineering,
Tel Aviv University, Tel Aviv 69978, Israel

Uwe Günther
Helmholtz Center Dresden-Rossendorf, POB 510119,
D-01314 Dresden, Germany

arXiv:1204.5530v2 [quant-ph] 18 Jun 2012

We introduce four basic two-dimensional (2D) plaquette configurations with onsite cubic nonlinearities, which may be used as building blocks for 2D $\mathcal{PT}$-symmetric lattices. For each configuration, we develop a dynamical model and examine its $\mathcal{PT}$ symmetry. The corresponding nonlinear modes are analyzed starting from the Hamiltonian limit, with zero value of the gain-loss coefficient, γ. Once the relevant waveforms have been identified (chiefly, in an analytical form), their stability is examined by means of linearization in the vicinity of stationary points. This reveals diverse and, occasionally, fairly complex bifurcations. The evolution of unstable modes is explored by means of direct simulations. In particular, stable localized modes are found in these systems, although the majority of identified solutions is unstable.

PACS numbers: 63.20.Pw, 05.45.Yv, 03.75.Lm, 03.65.Ca, 11.30.Er, 02.40.Xx, 02.20.Sv

I. INTRODUCTION

The theme of $\mathcal{PT}$ (parity–time) symmetric systems was initiated in the works of Bender and collaborators [1] as an alternative to the standard quantum theory, where the Hamiltonian is postulated to be Hermitian. The principal conclusion of these works was that $\mathcal{PT}$-invariant Hamiltonians, which are not necessarily Hermitian, may still give rise to completely real spectra, thus being appropriate for the description of physical settings. In terms of the Schrödinger-type Hamiltonians, which include the usual kinetic-energy operator and the potential term, $V(x)$, the $\mathcal{PT}$-invariance admits complex potentials, subject to constraint that $V^*(x) = V(-x)$.

Recent developments in optics have resulted in an experimental realization of the originally theoretical concept of the $\mathcal{PT}$-symmetric Hamiltonians, chiefly due to the work by Christodoulides and co-workers [2] (see also [3]). It has been demonstrated that the controllable imposition of symmetrically set and globally balanced gain and loss may render optical waveguiding arrays a fertile territory for the construction of $\mathcal{PT}$-symmetric complex potentials. The first two such realizations made use of couplers composed of two waveguides with and without loss [4] (so-called passive $\mathcal{PT}-$couplers), or, in more "standard" form, a pair of coupled waveguides, one carrying gain and the other one loss [5]. In fact, more general models of linearly coupled active (gain-carrying) and passive (lossy) intrinsically nonlinear waveguides, without imposing the condition of the gain-loss balance, were considered earlier, and stable solitons were found in them [6], including exact solutions [7] (see also a brief review in Ref. [8]). Recently, an electronic analog of such settings has also been implemented [9, 10]. Configurations with a hidden $\mathcal{PT}$ symmetry have been identified also in fine-tuned parameter regions of microwave billiards [11]. Effects of the nonlinearity in a Gross-Pitaevski equation on the $\mathcal{PT}$ properties of a Bose-Einstein condensate have been analyzed in [12]. The possibility to engineer $\mathcal{PT}$-symmetric *oligomers* (coupled complexes of a few loss-and gain-carrying elements) [13], which may include nonlinearity, was an incentive to a broad array of additional studies on both the few-site systems and entire $\mathcal{PT}$-symmetric lattices [14–21]. More recently, nonlinear $\mathcal{PT}$-symmetric systems, incorporating $\mathcal{PT}$-balanced nonlinear terms, have drawn considerable interest too [22]-[25].

Most of the $\mathcal{PT}$-invariant systems considered thus far have been one-dimensional (1D) in their nature, although the stability of solitons in 2D periodic $\mathcal{PT}$-symmetric potentials has also been recently investigated [26]. Actually, 2D arrays of optical waveguides can be readily built [27] (the same is true about other quasi-discrete systems, including electrical ones), hence, a natural question is whether $\mathcal{PT}$-symmetric oligomers (and ultimately lattices built of such building blocks) can be created in a 2D form. This work aims to make a basic step in this direction, by introducing fundamental 2D plaquettes consisting, typically, of four sites (in one case, it will be a five-site cross). These configurations, illustrated by Fig. 1, are inspired by earlier works on 2D Hamiltonian lattices described by discrete nonlinear

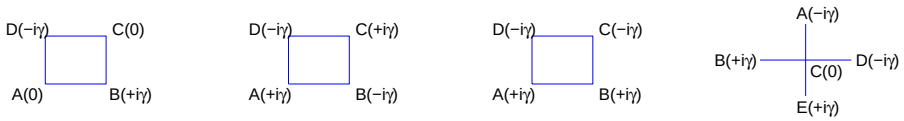

(a) mode 0+0- (b) mode +-+- (c) mode ++- - (d) mode +-0+-

FIG. 1: (Color online) The different fundamental plaquette configurations (i.e., two-dimensional *oligomers*) including the linear balanced gain and loss. Among these, (a), (c) and (d) are $\mathcal{PT}$-symmetric, while (b) is not in the strict sense, but it is interesting too, as an implementation of alternating gain and loss nodes in the plaquette pattern. The nodes are labeled so as to connect the gain-loss profiles to the evolution of individual nodes in dynamical simulations. The sets are coded by chains of symbols, with $+, -$ and 0 corresponding, respectively, to the linear gain, loss, or absence of either effect at particular sites.

Schrödinger equations [28], where diverse classes of modes, including discrete solitary vortices [29, 30], have been predicted and experimentally observed [31, 32]. The plaquettes proposed herein should be straightforwardly accessible with current experimental techniques in nonlinear optics, as a straightforward generalization of the coupler-based setting reported in Ref. [5]. We start from the well-established Hamiltonian form of such plaquettes in the conservative form, gradually turning on the gain-loss parameter (γ), as the strength of the $\mathcal{PT}$-invariant terms, to examine stationary states supported by the plaquettes, studying their stability against small perturbations and verifying the results through direct simulations. Actually, in this work we focus on those (quite diverse, although, obviously, not most generic) modes that can be found in an analytical form, while their stability is studied by means of numerical methods. The analytical calculations and the manifestations of interesting features, such as a potential persistence past the critical point of the linear $\mathcal{PT}$ symmetry, are enabled by the enhanced symmetry of the modes that we consider below. It is conceivable that additional asymmetric modes may exist too within these 2D configurations.

Our principal motivation for studying the above systems stems from the fact that realizations of $\mathcal{PT}$-symmetry e.g. within the realm of nonlinear optics will be inherently endowed with nonlinearity. Hence, it is only natural to inquire about the interplay of the above type of linear systems with the presence of nonlinear effects. In addition to this physical argument, there exists an intriguing mathematical one which concerns the existence, stability and dynamical fate of the nonlinear states in the presence of $\mathcal{PT}$-symmetric perturbations. In particular, previous works [12, 13, 18, 33, 34] point to the direction that neither the existence, nor the stability of $\mathcal{PT}$-symmetric nonlinear states mirrors that of their linear counterparts (or respects the phase transition of the latter generically). The presentation of our results is structured as follows. Section II contains a part of the analytical results, including a detailed analysis of the $\mathcal{PT}-$symmetry properties of the nonlinear Schrödinger type model, as well as the spectral properties of the linear Hamiltonian subsystems. Section III is devoted to the existence, stability and dynamics of stationary modes in the nonlinear systems. Beside analytical results, it contains a detailed presentation of the numerical findings. In section IV we summarize conclusions and discuss directions for future studies.

II. THE SETUP AND SYMMETRY PROPERTIES

A. General techniques

The dynamics of the 2D plaquettes that we are going to consider is described by a multicomponent nonlinear Schrödinger equation (NLSE)

$$i\dot{\mathbf{u}} = H_L\mathbf{u} + H_{NL}(\mathbf{u})\mathbf{u} \tag{1}$$

built over a transposition-symmetric linear $N \times N$ Hermitian matrix Hamiltonian $H_L = H_L^T$ and an additional nonlinear $N \times N$ matrix operator, $H_{NL}(\mathbf{u}) = H_{NL}^T(\mathbf{u})$. To understand the symmetry properties of this NLSE, we first analyze the associated linear problem

$$i\dot{\mathbf{u}} = H_L\mathbf{u}, \tag{2}$$

and check then whether the symmetry is preserved by the nonlinear term, $H_{NL}(\mathbf{u})\mathbf{u}$. The analysis can be built, in a part, on techniques developed for other nonlinear dynamical systems with symmetry preservation [35–42].

For the present setups, the time reversal operation $\mathbf{T}$ can be defined as the combined action of a scalar-type complex conjugation $\mathcal{T}$, $\mathcal{T}^2 = I$, and the sign change of time, $t \to -t$, in full accordance with Wigner's original work which

introduced these concepts [43]. For the linear Schrödinger equation (2) and its solutions

$$\begin{aligned} \mathbf{u}(t) &= \sum_{n=1}^{N} e^{-iE_n t}\mathbf{u}_n, \\ H_L\mathbf{u}_n &= E_n\mathbf{u}_n, \end{aligned} \tag{3}$$

this implies

$$\begin{aligned} \mathbf{T}(i\partial_t\mathbf{u}) &= \mathbf{T}(H_L\mathbf{u}), \\ i\partial_t\mathbf{T}(\mathbf{u}) &= \bar{H}_L\mathbf{T}(\mathbf{u}), \\ \mathbf{T}\mathbf{u}(t) &= \mathcal{T}\mathbf{u}(t)|_{t\to -t} = \sum_{n=1}^{N} e^{-i\bar{E}_n t}\bar{\mathbf{u}}_n\,, \end{aligned} \tag{4}$$

where the overbar denotes complex conjugation. From the actual form of the gain-loss arrangements in the 2D plaquettes we can conjecture the existence of certain plaquette-dependent parity operators $\mathcal{P}$, with $\mathcal{P}^2 = I$, which will render the Hamiltonians $\mathcal{PT}-$symmetric, $[\mathcal{PT}, H_L] = 0$. To find an explicit representation of these parity operators $\mathcal{P}$, we use the following ansatz,

$$\mathcal{P} \in \mathbb{R}^{N\times N}, \qquad [\mathbf{T}, \mathcal{P}] = 0 \tag{5}$$

together with the pseudo-Hermiticity condition

$$H_L^\dagger = \mathcal{P}H_L\mathcal{P}. \tag{6}$$

The latter follows trivially from Eq. (5), $[\mathcal{PT}, H_L] = 0$, and the transposition symmetry, $H_L = H_L^T$. These parity operators $\mathcal{P}$ will be used to check whether the corresponding nonlinear terms $H_{NL}(\mathbf{u})$ satisfy the same $\mathcal{PT}-$symmetry. In contrast to linear setups with the $\mathcal{PT}-$symmetry being either exact ($[\mathcal{PT}, H_L] = 0$, $\mathcal{P}\mathbf{T}\mathbf{u} \propto \mathbf{u}$) or spontaneously broken ($[\mathcal{PT}, H_L] = 0$, $\mathcal{P}\mathbf{T}\mathbf{u} \not\propto \mathbf{u}$), the nonlinear setups considered in the present paper allow for sectors of exact $\mathcal{PT}-$symmetry ($[\mathcal{PT}, H_{NL}(\mathbf{u})] = 0$, $\mathcal{P}\mathbf{T}\mathbf{u} \propto \mathbf{u}$) and of broken $\mathcal{PT}-$symmetry ($\mathcal{P}\mathbf{T}\mathbf{u} \not\propto \mathbf{u} \implies [\mathcal{PT}, H_{NL}(\mathbf{u})] \neq 0$), as it is common for nonlinear $\mathcal{PT}$-symmetric systems [22]-[25].

B. $\mathcal{PT}-$symmetry properties of 2D plaquettes

We start from the 2D plaquette of 0+0- type depicted as configuration (a) in Fig. 1. This plaquette has only two (diagonally opposite) nodes carrying the gain and loss, while the other two nodes bear no such effects. The corresponding dynamical equations for the amplitudes at the four sites of this oligomer are

$$\begin{aligned} i\dot{u}_A &= -k(u_B + u_D) - |u_A|^2 u_A, \\ i\dot{u}_B &= -k(u_A + u_C) - |u_B|^2 u_B + i\gamma u_B, \\ i\dot{u}_C &= -k(u_B + u_D) - |u_C|^2 u_C, \\ i\dot{u}_D &= -k(u_A + u_C) - |u_D|^2 u_D - i\gamma u_D, \end{aligned} \tag{7}$$

where $\gamma \in \mathbb{R}$ is the above-mentioned gain-loss coefficient, and $k \in \mathbb{R}$ is a real coupling constant. The nonlinearity coefficients are scaled to be 1 (we use time t as the evolution variable, although in the mathematically equivalent propagation equations for optical waveguides t has to be identified with the propagation distance, z).

Denoting $\mathbf{u} := (u_A, u_B, u_C, u_D)^T \in \mathbb{C}^4$, the matrices H_L and $H_{NL}(\mathbf{u})$ in (1) take the form of

$$\begin{aligned} H_L &= \begin{pmatrix} 0 & -k & 0 & -k \\ -k & i\gamma & -k & 0 \\ 0 & -k & 0 & -k \\ -k & 0 & -k & -i\gamma \end{pmatrix} = H_L^T, \\ &= -k(I + \sigma_x) \otimes \sigma_x + i\frac{\gamma}{2}\sigma_z \otimes (I - \sigma_z), \end{aligned} \tag{8}$$

$$H_{NL}(\mathbf{u}) = -\begin{pmatrix} |u_A|^2 & 0 & 0 & 0 \\ 0 & |u_B|^2 & 0 & 0 \\ 0 & 0 & |u_C|^2 & 0 \\ 0 & 0 & 0 & |u_D|^2 \end{pmatrix} = H_{NL}^T(\mathbf{u}) = H_{NL}^\dagger(\mathbf{u}). \tag{9}$$

To find the parity matrix $\mathcal{P}$ which renders the linear Hamiltonian $\mathcal{PT}-$symmetric, $[\mathcal{PT}, H_L] = 0$, we use the pseudo-Hermiticity condition (6) and notice that

$$\begin{aligned} H_L &= H_{L,0} + H_{L,1}, \\ H_{L,0} &= -k(I+\sigma_x)\otimes\sigma_x = H_{L,0}^\dagger, \\ H_{L,1} &= i\frac{\gamma}{2}\sigma_z\otimes(I-\sigma_z) = -H_{L,1}^\dagger. \end{aligned} \tag{10}$$

Obviously, the following relations should hold:

$$\begin{aligned} \mathcal{P}H_{L,0}\mathcal{P} = H_{L,0} \qquad &\Longrightarrow \qquad [\mathcal{P}, H_{L,0}] = 0 \\ \mathcal{P}H_{L,1}\mathcal{P} = -H_{L,1} \qquad &\Longrightarrow \qquad \{\mathcal{P}, H_{L,1}\} = 0. \end{aligned} \tag{11}$$

The first of these conditions together with $\mathcal{P}^2 = I$, $\mathcal{P} \neq I$ reduces the possible form of the parity transformation to one of the three types,

$$\mathcal{P}_{0x} := I\otimes\sigma_x\,, \qquad \mathcal{P}_{x0} := \sigma_x\otimes I\,, \qquad \mathcal{P}_{xx} := \sigma_x\otimes\sigma_x\,, \tag{12}$$

where $\sigma_{x,y,z}$ are the usual Pauli matrices. Taking into account that $\sigma_x\sigma_z\sigma_x = -\sigma_z$, the anti-commutativity condition in Eqs. (11) singles out the only possible parity matrix:

$$\mathcal{P} = \mathcal{P}_{x0} = \begin{pmatrix} 0 & I \\ I & 0 \end{pmatrix} = \begin{pmatrix} 0 & 0 & 1 & 0 \\ 0 & 0 & 0 & 1 \\ 1 & 0 & 0 & 0 \\ 0 & 1 & 0 & 0 \end{pmatrix} \tag{13}$$

for the linear transformation, i.e., the matrix interchanging A and C, as well as B and D. One then immediately checks that

$$H_{NL}(\mathcal{P}\mathbf{u}) = \mathcal{P}H_{NL}(\mathbf{u})\mathcal{P} = -\begin{pmatrix} |u_C|^2 & 0 & 0 & 0 \\ 0 & |u_D|^2 & 0 & 0 \\ 0 & 0 & |u_A|^2 & 0 \\ 0 & 0 & 0 & |u_B|^2 \end{pmatrix} \neq H_{NL}^\dagger(\mathbf{u}). \tag{14}$$

Hence, in contrast to the linear component H_L, the nonlinear terms $H_{NL}(\mathbf{u})$ corresponding to Eqs. (7) are not $\mathcal{PT}-$symmetric, in the usual matrix sense. Rather, the symmetry properties of the nonlinear terms have to be considered in the context of the nonlinear Schrödinger equation itself. Acting with $\mathcal{PT}$ on Eq. (1) we observe that

$$\begin{aligned} \mathcal{PT}(i\partial_t\mathbf{u}) &= \mathcal{PT}\left[H_L\mathbf{u} + H_{NL}(\mathbf{u})\mathbf{u}\right], \\ i\partial_t(\mathcal{PT}\mathbf{u}) &= H_L\mathcal{PT}\mathbf{u} + H_{NL}(\mathcal{PT}\mathbf{u})(\mathcal{PT}\mathbf{u}). \end{aligned} \tag{15}$$

Hence, the full NLSE system (7) remains invariant if we define the $\mathcal{PT}$ transformation of the vectorial wave function obeying this system as follows:

$$\begin{aligned} \mathcal{PT}\mathbf{u} &= e^{i\phi}\mathbf{u}, \qquad \phi\in\mathbb{R} \\ \mathcal{P}\bar{\mathbf{u}}(-t) &= e^{i\phi}\mathbf{u}(t). \end{aligned} \tag{16}$$

This is in full analogy to the condition of exact $\mathcal{PT}-$symmetry for the corresponding linear Schrödinger equation[1]. But the condition of *spontaneously broken* $\mathcal{PT}-$symmetry ($[\mathcal{PT}, H_L] = 0$, $\mathcal{PT}\mathbf{u} \not\propto \mathbf{u}$) is replaced by the condition of *completely broken* $\mathcal{PT}-$symmetry ($\mathcal{PT}\mathbf{u} \not\propto \mathbf{u} \implies [\mathcal{PT}, H_{NL}(\mathbf{u})] \neq 0$). In contrast to the present 2D plaquettes, which are mainly motivated by feasible experimental realizations, one can envision more sophisticated setups with $\mathcal{P}H_{NL}(\mathbf{u})\mathcal{P} = H_{NL}^\dagger(\mathbf{u})$. This will lead to a new type of partial (or intermediate) $\mathcal{PT}-$symmetry (to be considered elsewhere), which for solutions $\mathbf{u}(t)$ with broken $\mathcal{PT}-$symmetry will keep the nonlinear term $H_{NL}(\mathbf{u})$ explicitly

[1]) We note that apart from trivial stationary type solutions with factorizing structure $\mathbf{u}(t) = e^{-iEt}\mathbf{u}_0$, nonlinearity matrices $H_{NL}(\mathbf{u})$ of more general type than that in (9) and (14) may be envisioned which may produce $\mathcal{PT}-$symmetric solutions $\mathbf{u}(t)$ with less simple time dependence. A detailed analysis of such systems will be presented elsewhere.

$\mathcal{PT}-$symmetric ($\mathcal{P}-$pseudo-Hermitian) in the matrix sense, but not $\mathcal{PT}-$symmetric (under inclusion of the explicit time reversal $t \to -t$) in the sense of the NLSE system.

For configurations (b) and (c) in Fig. 1, $H_{L,0}$ and $H_{NL}(\mathbf{u})$ are still given by Eqs. (8) and (10), but with

$$H_{L,1} = \begin{pmatrix} i\gamma & 0 & 0 & 0 \\ 0 & -i\gamma & 0 & 0 \\ 0 & 0 & i\gamma & 0 \\ 0 & 0 & 0 & -i\gamma \end{pmatrix} = i\gamma I \otimes \sigma_z, \tag{17}$$

$$H_{L,1} = \begin{pmatrix} i\gamma & 0 & 0 & 0 \\ 0 & i\gamma & 0 & 0 \\ 0 & 0 & -i\gamma & 0 \\ 0 & 0 & 0 & -i\gamma \end{pmatrix} = i\gamma \sigma_z \otimes I \tag{18}$$

respectively. Hence, relations (11) are valid for both configurations (b) and (c) as well. Using (12) in $\mathcal{P}H_{L,1}\mathcal{P} = -H_{L,1}$, we find a richer variety of parity operators $\mathcal{P}$ than for configuration (a). Configuration (b) allows for

$$\mathcal{P}_{0x} = \begin{pmatrix} \sigma_x & 0 \\ 0 & \sigma_x \end{pmatrix}, \qquad \mathcal{P}_{xx} = \begin{pmatrix} 0 & \sigma_x \\ \sigma_x & 0 \end{pmatrix}, \tag{19}$$

whereas configuration (c) may be associated with

$$\mathcal{P}_{x0} = \begin{pmatrix} 0 & I \\ I & 0 \end{pmatrix}, \qquad \mathcal{P}_{xx} = \begin{pmatrix} 0 & \sigma_x \\ \sigma_x & 0 \end{pmatrix}. \tag{20}$$

For configuration (d), we have

$$H_{L,0} = \begin{pmatrix} 0 & 0 & -k & 0 & 0 \\ 0 & 0 & -k & 0 & 0 \\ -k & -k & 0 & -k & -k \\ 0 & 0 & -k & 0 & 0 \\ 0 & 0 & -k & 0 & 0 \end{pmatrix}, \tag{21}$$

$$H_{L,1} = \begin{pmatrix} -i\gamma & 0 & 0 & 0 & 0 \\ 0 & i\gamma & 0 & 0 & 0 \\ 0 & 0 & 0 & 0 & 0 \\ 0 & 0 & 0 & -i\gamma & 0 \\ 0 & 0 & 0 & 0 & i\gamma \end{pmatrix}, \tag{22}$$

$$H_{NL}(\mathbf{u}) = -\begin{pmatrix} |u_A|^2 & 0 & 0 & 0 & 0 \\ 0 & |u_B|^2 & 0 & 0 & 0 \\ 0 & 0 & |u_C|^2 & 0 & 0 \\ 0 & 0 & 0 & |u_D|^2 & 0 \\ 0 & 0 & 0 & 0 & |u_E|^2 \end{pmatrix}, \tag{23}$$

and simple computer algebra gives again two possible parity operators:

$$\mathcal{P}_{d,0} = \begin{pmatrix} 0 & 1 & 0 & 0 & 0 \\ 1 & 0 & 0 & 0 & 0 \\ 0 & 0 & 1 & 0 & 0 \\ 0 & 0 & 0 & 0 & 1 \\ 0 & 0 & 0 & 1 & 0 \end{pmatrix}, \quad \mathcal{P}_{d,x} = \begin{pmatrix} 0 & 0 & 0 & 0 & 1 \\ 0 & 0 & 0 & 1 & 0 \\ 0 & 0 & 1 & 0 & 0 \\ 0 & 1 & 0 & 0 & 0 \\ 1 & 0 & 0 & 0 & 0 \end{pmatrix}, \tag{24}$$

in strong structural analogy to configuration (b). One verifies that $H_{NL}(\mathcal{P}\mathbf{Tu}) = \mathcal{P}H_{NL}(\mathbf{u})\mathcal{P} \neq H_{NL}^{\dagger}(\mathbf{u})$ holds also for configurations (b), (c) and (d), hence all 2D plaquettes considered in the present paper are not $\mathcal{PT}-$symmetric in the usual matrix sense.

C. Spectral behavior of associated linear setups

Next, we turn to the eigenvalue problems of the linear setups associated with plaquettes (a) - (d), i.e., to solutions of the equation

$$H_L \mathbf{u}_n = E_n \mathbf{u}_n. \tag{25}$$

From the corresponding characteristic polynomials, $\det(H_L - EI) = 0$,

$$\begin{aligned}
&\text{(a)}: && E^2\left[E^2-(4k^2-\gamma^2)\right]=0,\\
&\text{(b)}: && (E^2+\gamma^2)\left[E^2-(4k^2-\gamma^2)\right]=0,\\
&\text{(c)}: && E^4-2(2k^2-\gamma^2)E^2+\gamma^4=0,\\
&\text{(d)}: && E(E^2+\gamma^2)\left[E^2-(4k^2-\gamma^2)\right]=0,
\end{aligned} \tag{26}$$

we find

$$\begin{aligned}
&\text{(a)}: && E_{1,2}=0, \qquad E_{3,4}=\pm\sqrt{4k^2-\gamma^2}\\
&\text{(b)}: && E_{1,2}=\pm i\gamma, \qquad E_{3,4}=\pm\sqrt{4k^2-\gamma^2}\\
&\text{(c)}: && E_{1,2}=\sqrt{2k^2-\gamma^2\pm 2k\sqrt{k^2-\gamma^2}}\\
& && E_{3,4}=-\sqrt{2k^2-\gamma^2\pm 2k\sqrt{k^2-\gamma^2}}\\
&\text{(d)}: && E_{1,2}=\pm i\gamma, \qquad E_{3,4}=\pm\sqrt{4k^2-\gamma^2}, \qquad E_5=0.
\end{aligned} \tag{27}$$

Obviously, the matrix Hamiltonians H_L for plaquettes (a) and (d) are not of full rank. For plaquette (a) we find $\text{rank}\,(H_L)=2$, and H_L has a two-dimensional kernel space, $\ker(H_L)=\text{span}_{\mathbb{C}}(\mathbf{u}_1,\mathbf{u}_2)$. For plaquette (d) we find $\text{rank}\,(H_L)=4$ and $\ker(H_L)=\mathbb{C}^*\times\mathbf{u}_5$, where $\mathbb{C}^*=\mathbb{C}-\{0\}$. Moreover, we see that the spectrum for plaquette (d), up to the additional eigenvalue $E_5=0$, coincides with that for (b). The different eigenvalues of the 4-node plaquettes displayed in Eqs. (27) show that these plaquettes are also physically not equivalent. Equivalence classes of nonlinear 4-node plaquettes with isospectral linear Hamiltonians H_L but different pairwise couplings have been considered, e.g., in [33]. For plaquettes (a), (b) and (d) an exceptional point (EP) occurs at $\gamma^2=4k^2$, being associated with a branching of the eigenvalue pair $E_{3,4}$

$$\begin{aligned}
E_{3,4}&\in\mathbb{R} \qquad &&\text{for} \qquad 4k^2\geq\gamma^2\\
E_{3,4}&\in i\mathbb{R} \qquad &&\text{for} \qquad 4k^2<\gamma^2.
\end{aligned} \tag{28}$$

In the case of plaquette (a), all four eigenvalues are involved in the branching at $\gamma=\pm 2k$, where $E_1=\ldots=E_4=0$. Via Jordan decomposition (e.g., with the help of the corresponding linear algebra tool of Mathematica) we find that

$$(a): \qquad H_L(\gamma=\pm 2k)\sim\begin{pmatrix}0&1&0&0\\0&0&1&0\\0&0&0&0\\0&0&0&0\end{pmatrix}=J_3(0)\oplus J_1(0), \tag{29}$$

i.e., a spectral degeneration of the type $(0^3,0^1)$ in Arnold's notation [44], or, in other words, a third-order EP with a single decoupled fourth mode. Hence, plaquettes of type (a) may serve as an easily implementable testground for the experimental investigation of third-order EPs (see e.g. [45–48]). For plaquettes (b) and (d) we have second-order EPs at $\gamma^2=4k^2$, similar as for plaquette (c) where a pair of second-order EPs occurs at $\gamma^2=k^2$ with $E_1=E_2=|k|$, $E_3=E_4=-|k|$.

From the eigenvalues in (27) we read off the $\mathcal{PT}-$symmetry content of the four types of plaquettes. The sector of exact $\mathcal{PT}-$symmetry (i.e., the sector with all eigenvalues purely real, $E_n\in\mathbb{R},\ \forall n$) corresponds to

$$\begin{aligned}
&\text{(a)}: && \gamma^2\leq 4k^2,\\
&\text{(b)}: && \gamma=0,\\
&\text{(c)}: && \gamma^2\leq k^2,\\
&\text{(d)}: && \gamma=0,
\end{aligned} \tag{30}$$

i.e., for plaquettes (b) and (d) the $\mathcal{PT}-$symmetry is spontaneously broken as soon as the gain-loss coupling is switched on, namely for $\gamma\neq 0$.

III. EXISTENCE, STABILITY AND DYNAMICS OF NONLINEAR STATES

In this section, we seek stationary solutions of the type

$$\mathbf{u}_0(t)=e^{-iEt}\mathbf{u}_0, \qquad E\in\mathbb{R}, \qquad \mathbf{u}_0=(a,b,c,d)^T\in\mathbb{C}^4 \tag{31}$$

constructed over constant vectors $\mathbf{u}_0$. According to (15) and (16) such solutions will be $\mathcal{PT}-$symmetric provided it holds $\mathcal{PT}\mathbf{u}_0 = e^{i\varphi}\mathbf{u}_0$ for some $\varphi \in \mathbb{R}$. We will test these symmetry properties for the solutions to be obtained. We note that restricting the explicit analysis to stationary solutions of the type (31) we by construction exclude from this analysis $\mathcal{PT}-$violating solutions with $E \notin \mathbb{R}$ which are necessarily non-stationary.

A useful technical tool to facilitate the explicit derivation of stationary solutions $\mathbf{u}_0(t)$ are conservation equations of the type

$$\partial_t(\mathbf{u}^\dagger Y \mathbf{u}) = i\mathbf{u}^\dagger \left(H^\dagger Y - YH\right)\mathbf{u}, \tag{32}$$

constructed from Eq. (1) and its adjoint, where Y denotes an arbitrary constant matrix. The most simplest of them can be found via Eqs. (6), (8) and Eq. (10) to be

$$\partial_t|\mathbf{u}|^2 = \partial_t(\mathbf{u}^\dagger\mathbf{u}) \;=\; -2i\mathbf{u}^\dagger H_{L,1}\mathbf{u} \tag{33}$$

$$\partial_t(\mathbf{u}^\dagger\mathcal{P}\mathbf{u}) \;=\; i\mathbf{u}^\dagger\left[H^\dagger_{NL}(\mathbf{u})\mathcal{P} - \mathcal{P}H_{NL}(\mathbf{u})\right]\mathbf{u}. \tag{34}$$

For stationary equations $\mathbf{u}_0(t)$ the time-dependent phase factors e^{-iEt} cancel so that the left-hand-sides of these relations vanish, yielding simple algebraic constraints on the right-hand-sides. From Eq. (34) we see that for stationary solutions the $\mathcal{PT}$ inner product[2] will remain conserved ($\mathbf{u}^\dagger\mathcal{P}\mathbf{u}$ =const) regardless of the violated $\mathcal{P}-$pseudo-Hermiticity, $\mathcal{P}H^\dagger_{NL}(\mathbf{u})\mathcal{P} \neq H_{NL}(\mathbf{u})$, characteristic for of our specific nonlinear plaquette couplings (see Eq. (14)).

Subsequently, we first derive classes of stationary solutions $\mathbf{u}_0(t)$ explicitly. Then, we analyze the stability of small perturbations over these stationary solutions by the linearization, via ansatz

$$\mathbf{u}(t) = e^{-iEt}\left[\mathbf{u}_0 + \delta(e^{\lambda t}r + e^{\bar{\lambda}t}s)\right] + O(\delta^2), \qquad |\delta| \ll 1, \tag{35}$$

where δ is the small amplitude of the perturbation. Exponents λ can be defined as Wick-rotated eigenvalues from the corresponding 8×8 perturbation matrix $\mathbf{B}$ (see, e.g., [28] for more details):

$$\begin{aligned}(\mathbf{B} - i\lambda I_8)\mathbf{x} \;&=\; 0\\ \mathbf{B} := \quad &\begin{pmatrix} \partial_{u_n}F(\mathbf{u},\bar{\mathbf{u}}) & \partial_{\bar{u}_n}F(\mathbf{u},\bar{\mathbf{u}}) \\ -\partial_{u_n}\bar{F}(\mathbf{u},\bar{\mathbf{u}}) & -\partial_{\bar{u}_n}\bar{F}(\mathbf{u},\bar{\mathbf{u}})\end{pmatrix}, \qquad n = 1,2,3,4\\ \mathbf{x} \;&=\; (r,\bar{s})^T,\end{aligned} \tag{36}$$

where

$$F(\mathbf{u},\bar{\mathbf{u}}) := [H(\mathbf{u}) - E]\mathbf{u} \tag{37}$$

characterizes the stationary problem, and the elements of the matrix $\mathbf{B}$ are evaluated at $\mathbf{u} = \mathbf{u}_0$. Linear stability is ensured for $\lambda \in i\mathbb{R}$, whereas $\lambda \notin i\mathbb{R}$ corresponds to growing and decaying modes, i.e., exponential instabilities.

A. The plaquette of the 0+0- type

Substituting ansatz (31) for the stationary solutions in Eqs. (1), (33) and (34) we obtain the following algebraic equations:

$$\begin{aligned} Ea \;&=\; k(b+d) + |a|^2a,\\ Eb \;&=\; k(a+c) + |b|^2b - i\gamma b,\\ Ec \;&=\; k(b+d) + |c|^2c,\\ Ed \;&=\; k(a+c) + |d|^2d + i\gamma d,\end{aligned} \tag{38}$$

[2]) For completeness, we note that in the context of $\mathcal{PT}$ quantum mechanics (PTQM) the $\mathcal{PT}$ inner product was introduced first by Znojil in [49] in 2001. Immediately afterwards, it was interpreted by Japaridze as indefinite inner product [50] in a Krein space and generalized by Mostafazadeh to the $\eta-$metric in the context of pseudo-Hermitian Hamiltonians [51]. Finally, it was used by Bender, Brody and Jones in 2002 to construct the positive definite $\mathcal{CPT}$ inner product [52]. For oligomer settings (of plaquettes or other few site configurations), it can be employed, e.g., to derive a simple algebraic constraint or as a criterion of the numerical accuracy of the evolutionary dynamics (especially since the solutions rapidly acquire very large amplitudes when unstable, as will be seen below). It also turned out useful in [33].

$$\begin{aligned} \partial_t |\mathbf{u}|^2 &= -2i\mathbf{u}^\dagger H_{L,1}\mathbf{u}, \\ 0 &= 2\gamma(|b|^2 - |d|^2), \end{aligned} \tag{39}$$

and

$$\begin{aligned} \partial_t(\mathbf{u}^\dagger \mathcal{P}\mathbf{u}) &= i\mathbf{u}^\dagger \left[H_{NL}^\dagger(\mathbf{u})\mathcal{P} - \mathcal{P}H_{NL}(\mathbf{u})\right]\mathbf{u}, \\ 0 &= \left(|a|^2 - |c|^2\right)(\bar{a}c - \bar{c}a) + \left(|b|^2 - |d|^2\right)(\bar{b}d - \bar{d}b). \end{aligned} \tag{40}$$

These equations can be analyzed via the Madelung substitution (i.e., via amplitude-phase decomposition),

$$a = Ae^{i\phi_a}, b = Be^{i\phi_b}, c = Ce^{i\phi_c}, d = De^{i\phi_d}. \tag{41}$$

Without loss of generality, we may fix $\phi_a = 0$.

For arbitrary phase factors in (41), Eqs. (39) and (40) are satisfied by $A = C$ and $B = D$. Using this condition in Eq. (38) and dividing each equation (38) by the phase factor on its left-hand side, one obtains the imaginary parts of the resulting equations:

$$\begin{aligned} 0 &= kB\left[\sin(\phi_b - \phi_a) + \sin(\phi_d - \phi_a)\right] = 2kB\sin\left(\frac{\phi_b + \phi_d}{2} - \phi_a\right)\cos\left(\frac{\phi_b - \phi_d}{2}\right), \\ \gamma B &= kA\left[\sin(\phi_a - \phi_b) + \sin(\phi_c - \phi_b)\right] = 2kA\sin\left(\frac{\phi_a + \phi_c}{2} - \phi_b\right)\cos\left(\frac{\phi_a - \phi_c}{2}\right), \\ 0 &= kB\left[\sin(\phi_b - \phi_c) + \sin(\phi_d - \phi_c)\right] = 2kB\sin\left(\frac{\phi_b + \phi_d}{2} - \phi_c\right)\cos\left(\frac{\phi_b - \phi_d}{2}\right), \\ -\gamma B &= kA\left[\sin(\phi_a - \phi_d) + \sin(\phi_c - \phi_d)\right] = 2kA\sin\left(\frac{\phi_a + \phi_c}{2} - \phi_d\right)\cos\left(\frac{\phi_a - \phi_c}{2}\right). \end{aligned} \tag{42}$$

For $\phi_a = 0$ the first of these equations implies $\sin(\phi_b) = -\sin(\phi_d)$, hence either $\phi_b = -\phi_d$ (case 1) or $\phi_d = \phi_b - \pi$ (case 2). In case 1, we conclude from the third equation that either $\phi_b \neq \pm\pi/2$ and $\phi_c = 0$ (case 1a), or $\phi_b = \pm\pi/2$ and ϕ_c is arbitrary (case 1b). In case 2 the third equation is satisfied automatically. In all the three cases, the second and the fourth equation are compatible. They give

$$\begin{aligned} &\text{case 1a:} && \sin(\phi_b) = -\frac{\gamma B}{2kA}, \qquad \phi_c = 0, \qquad \phi_d = -\phi_b, \\ &\text{case 1b:} && \cos(\phi_c) = \mp\frac{\gamma B}{kA} - 1, \qquad \phi_d = -\phi_b = \mp\pi/2, \\ &\text{case 2:} && \sin(\phi_b) + \sin(\phi_b - \phi_c) = -\frac{\gamma B}{kA}, \qquad \phi_d = \phi_b - \pi. \end{aligned} \tag{43}$$

Returning to the phase-factor divided equations (38) and considering their real parts, we find

$$\begin{aligned} EA &= kB\left[\cos(\phi_b - \phi_a) + \cos(\phi_d - \phi_a)\right] + A^3, \\ EB &= kA\left[\cos(\phi_a - \phi_b) + \cos(\phi_c - \phi_b)\right] + B^3, \\ EA &= kB\left[\cos(\phi_b - \phi_c) + \cos(\phi_d - \phi_c)\right] + A^3, \\ EB &= kA\left[\cos(\phi_a - \phi_d) + \cos(\phi_c - \phi_d)\right] + B^3. \end{aligned} \tag{44}$$

The pairwise compatibility of the first and third, as well as of the second and fourth equations requires

$$\begin{aligned} \cos(\phi_b - \phi_a) + \cos(\phi_d - \phi_a) &= \cos(\phi_b - \phi_c) + \cos(\phi_d - \phi_c), \\ \cos(\phi_a - \phi_b) + \cos(\phi_c - \phi_b) &= \cos(\phi_a - \phi_d) + \cos(\phi_c - \phi_d). \end{aligned} \tag{45}$$

For case 1a, these conditions are trivially satisfied, whereas for the remaining cases they lead to further restrictions:

$$\begin{aligned} &\text{case 1b:} && \phi_c = 0; \pi \quad \Longrightarrow \quad && \gamma = \mp\frac{2kA}{B}; \\ & && && \gamma = 0; \\ &\text{case 2:} && && \phi_c = 2\phi_b \pm \pi, \quad \sin(\phi_b) = -\frac{\gamma B}{2kA}. \end{aligned} \tag{46}$$

In this way the phase angles are fixed for all the three cases and we can turn to the amplitudes. The corresponding equation sets reduce to

$$\begin{aligned} \text{case 1a:} \qquad EA &= 2kB\cos(\phi_b) + A^3, \\ EB &= 2kA\cos(\phi_b) + B^3, \\ \text{case 1b,2:} \qquad E &= A^2 = B^2. \end{aligned} \tag{47}$$

In the latter two cases (1b and 2) the amplitudes and phases completely decouple and we have

$$A = B = C = D = \sqrt{|E|}. \tag{48}$$

Case 1a allows for a richer behavior. Equating the terms $2k\cos(\phi_b)$ in the upper two equations (47) leads to the constraint

$$A^2(E - A^2) = B^2(E - B^2), \tag{49}$$

which can be resolved by $A = B$ (case 1aa) as well as by $E = A^2 + B^2$ (case 1ab). The analysis of these two cases can be completed with the help of the relation $\cos(\phi_b) = \pm\sqrt{1 - \dfrac{\gamma^2 B^2}{4k^2 A^2}}$ from Eq. (43).

As result we obtain the following set of stationary solutions:

$$\text{case 1a:} \qquad \sin(\phi_b) = -\frac{\gamma B}{2kA}, \qquad \phi_c = 0, \qquad \phi_d = -\phi_b,$$

$$\text{case 1aa:} \qquad A = B = C = D = \sqrt{E \mp \sqrt{4k^2 - \gamma^2}}, \tag{50}$$

$$\text{case 1ab:} \qquad A = C,\ B = D = \frac{2kA}{\sqrt{A^4 + \gamma^2}}, \quad E = A^2 + B^2, \tag{51}$$

$$\text{case 1b:} \qquad \phi_d = -\phi_b = \mp\pi/2, \quad \phi_c = 0, \pi, \qquad \gamma = \pm 2k, \quad \gamma = 0,$$

$$A = B = C = D = \sqrt{E}, \tag{52}$$

$$\text{case 2:} \qquad \sin(\phi_b) = -\frac{\gamma}{2k}, \qquad \phi_d = \phi_b - \pi, \qquad \phi_c = 2\phi_b \pm \pi,$$

$$A = B = C = D = \sqrt{E}. \tag{53}$$

From Eq. (40), it can also be seen that either $A = C$ or if $A \neq C$, then $\sin(\phi_a - \phi_c) = 0$ must be true. Here, we use the information available so far to check the $\mathcal{PT}-$symmetry content of the solutions (50) - (53) explicitly. For stationary solutions $\mathbf{u}(t) = e^{-iEt}\mathbf{u}_0$, $E \in \mathbb{R}$ the $\mathcal{PT}-$symmetry condition (16) implies

$$\mathcal{PT}\mathbf{u}_0 = e^{i\phi}\mathbf{u}_0. \tag{54}$$

Taking into account that $\mathcal{T}$ acts as complex conjugation, we see from the explicit structure of $\mathcal{P} = \mathcal{P}_{x0}$ in Eq. (13) that a stationary solution is $\mathcal{PT}-$symmetric if, with $\phi_a = 0$, it has $\phi_c = 0$ and $\phi_d = -\phi_b$ (up to a common phase shift). Additionally, the amplitudes have to coincide pairwise: $A = C$, $B = D$. For Eqs. (50) - (53) this means that all case-1 stationary solutions with $\phi_c = 0$ are $\mathcal{PT}-$symmetric in their present form. The case-2 mode becomes explicitly $\mathcal{PT}-$symmetric after a global $U(1)$ multiplication by a phase factor:

$$\begin{aligned} \mathbf{u}_0 &= e^{i(\phi_b - \pi/2)}\mathbf{v}_0, \\ \mathbf{v}_0 :=& \quad A\left[e^{-i(\phi_b - \pi/2)}, e^{i\pi/2}, e^{i(\phi_b - \pi/2)}, e^{-i\pi/2}\right]^T, \\ \mathcal{PT}\mathbf{v}_0 &= \mathbf{v}_0, \end{aligned} \tag{55}$$

where $\phi_c = 2\phi_b - \pi$ has to be chosen in Eq. (53). We note that this procedure is effectively equivalent to a redefinition of the original phase constraint: $\phi_a = 0 \ \mapsto \ \phi_a = -\phi_b + \pi/2$ at the very beginning of the calculations in Eq. (41).

The linear stability analysis was performed numerically. Subsequently we present corresponding graphical results. The plaquettes (b) - (d) can be analyzed in a similar way. For brevity's sake, in Fig. III A we present only the basic numerical results, by means of the following symbols:

- case 1aa with $A = B = C = D = \sqrt{E + \sqrt{4k^2 + \gamma^2}}$ — blue circles;

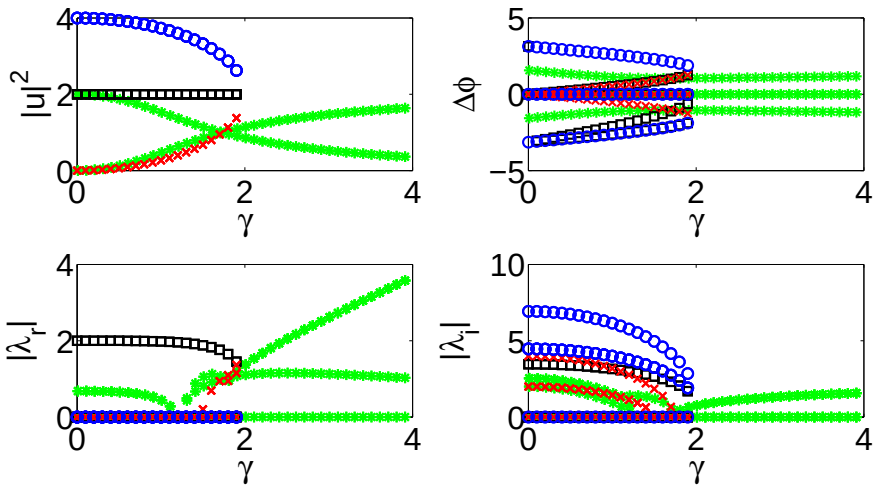

FIG. 2: (Color online) Profiles of the solutions for plaquette (a) from Fig. 1, with $E = 2$ and $k = 1$. Four different branches of the solutions are denoted by blue circles, red crosses, black squares and green stars. The top left and right panel display, respectively, the squared absolute values of the amplitudes and phase differences between adjacent sites for the respective states. The bottom left and right panels show real (the instability growth rates) and imaginary (oscillation frequencies) parts of the eigenvalues produced by the linearization around the stationary states. The continuations are shown versus the gain-loss parameter γ.

- case 1aa with $A = B = C = D = \sqrt{E - \sqrt{4k^2 - \gamma^2}}$ — red crosses;
- case 1ab — green stars;
- case 2 — black squares;
- Case 1b is not depicted explicitly because it corresponds to point configurations without gain-loss ($\gamma = 0$) and to exceptional point configurations $\gamma = \pm 2k$.

Figure III A presents the mode branches (their amplitudes, phases, and also their stability) over the gain-loss parameter γ, starting from the conservative system at $\gamma = 0$. The same symbols are used in Fig. 3, which displays typical examples of the spectral plane (λ_r, λ_i) for stability eigenvalues $\lambda = \lambda_r + i\lambda_i$ of the linearization; recall that the modes are unstable if they give rise to $\lambda_r \neq 0$. Explicitly we observe the following behavior.

- case 1aa with $A = B = C = D = \sqrt{E + \sqrt{4k^2 + \gamma^2}}$ — blue circles
  According to Fig. 3, the present solution is stable. Notice that, although featuring a phase profile, it cannot be characterized as a vortex state (the same is true for some other configurations carrying phase structure). Interestingly, the relevant configuration is generically stable bearing two imaginary pairs of eigenvalues.

- case 1aa with $A = B = C = D = \sqrt{E - \sqrt{4k^2 - \gamma^2}}$ — red crosses.
  Obviously, this kind of solutions as well as the previous one exist up to the exceptional point $\gamma = \pm 2k$ of the $\mathcal{PT}$-symmetry breaking in the linear system, where the two branches collide and disappear (leave the stationary regime and become nonstationary). As seen in Fig. 3, the present branch has two eigenvalue pairs which are purely imaginary for small γ, but become real (rendering the configuration unstable) at $\gamma = 1.49$ and then $\gamma = 1.73$, respectively. Ultimately, these pairs of unstable eigenvalues collide at the origin of the spectral plane with those of the previous branch (blue circles).

- case 1ab — green stars.
  This stationary solution has a number of interesting features. Firstly, it is the only one among the considered branches which has two unequal amplitudes. Secondly, it exists past the critical point $\gamma = \pm 2k$ of the linear system, due to the effect of the nonlinearity (the extension of the existence region for nonlinear modes was earlier found in 1D couplers [22] and oligomers [13, 33]). Furthermore, this branch has three non-zero pairs of stability eigenvalues, two of which form a quartet for small values of the gain-loss parameter, while the third

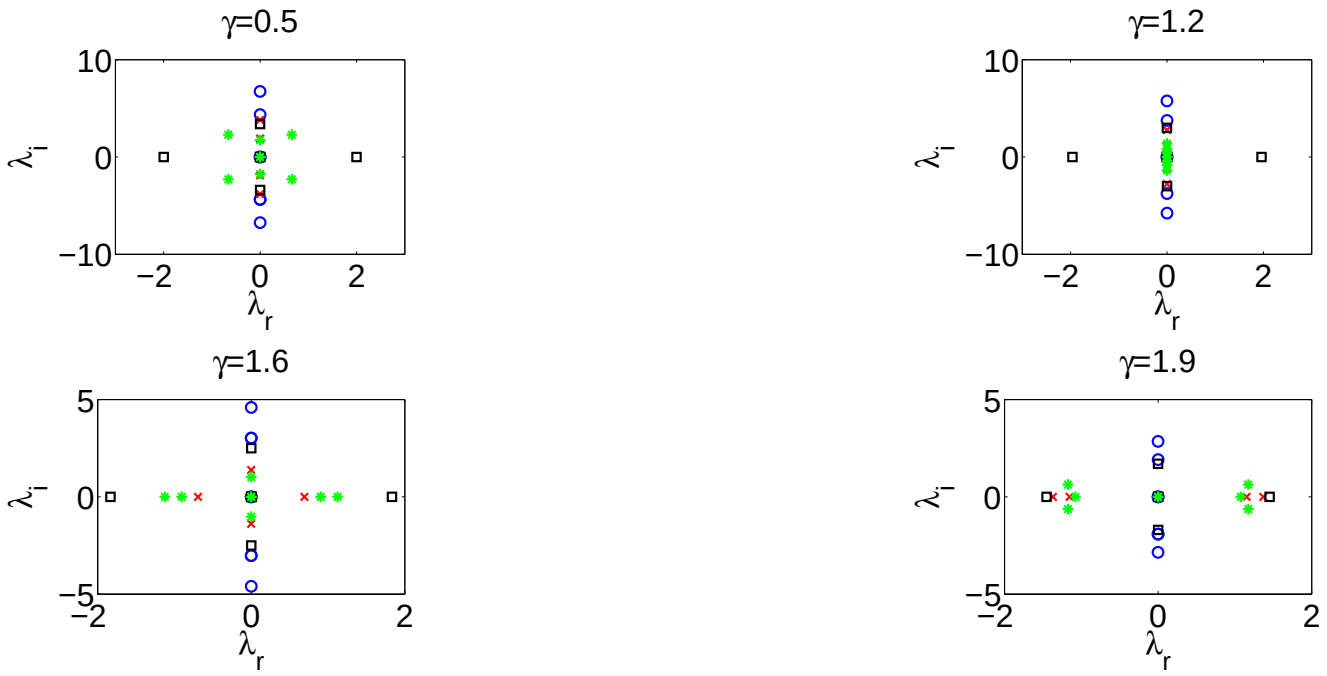

FIG. 3: (Color online) The stability plots for plaquette (a) from Fig. 1 with $E = 2$ and $k = 1$, for different values of γ. The notation for different branches is the same as in the previous figure. All branches are shown for $\gamma = 0.5$, $\gamma = 1.2$, $\gamma = 1.6$, and $\gamma = 1.9$ (top left, top right, bottom left, and bottom right panels, respectively).

is imaginary (i.e., the configuration is unstable due to the real parts of the eigenvalues within the quartet). At $\gamma = 1.17$, the eigenvalues of the complex quartet collapse into two imaginary pairs, rendering the configuration stable, in a narrow parametric interval. At $\gamma = 1.24$, the former imaginary pair becomes real, destabilizing the state again, while subsequent bifurcations of imaginary pairs into real ones occur at $\gamma = 1.28$ and $\gamma = 1.74$ (at the latter point, all three non-zero pairs are real). Shortly thereafter, two of these pairs collide at $\gamma = 1.76$ and rearrange into a complex quartet, which exists along with the real pair past that point.

- case 2 — black squares. In contrast to all other branches, this one is *always* unstable. One of the two nonzero eigenvalue pairs is always real (while the other is always imaginary), as seen in Fig. 3. This branch also terminates at the exceptional point $\gamma = \pm 2k$, as relation $\sin(\phi_b) = -\gamma/(2k)$ cannot hold at $|\gamma| > |2k|$. This branch collides with the two previous ones via a very degenerate bifurcation (that could be dubbed a "double saddle-center" bifurcation), which involves 3 branches instead of two as in the case of the generic saddle-center bifurcation, and two distinct eigenvalue pairs colliding at the origin of the spectral plane.

By means of direct simulations, we have also examined the dynamics of the modes belonging to different branches in Fig. 4. The stable blue-circle branch demonstrates only oscillations under perturbations. This implies that, despite the presence of the gain-loss profile, none of the perturbation eigenmodes grows in this case. Nevertheless, the three other branches ultimately manifest their dynamical instability, which is observed through the growth of the amplitude at the gain-carrying site [B, in Fig. 1(a)] at the expense of the lossy site (D). That is, the amplitude of the solution at the site with the gain grows, while the amplitude of the solution at the dissipation site loses all of its initial power. Depending on the particular solution, passive sites (the ones without gain or loss, such as A and C) may be effectively driven by the gain (as in the case of the black-square-branch, where the site A is eventually amplified due to the growth of the amplitude at site B) or by the loss (red-cross and green-star branches, where, eventually, the amplitudes at both A and C sites lose all of their optical power).

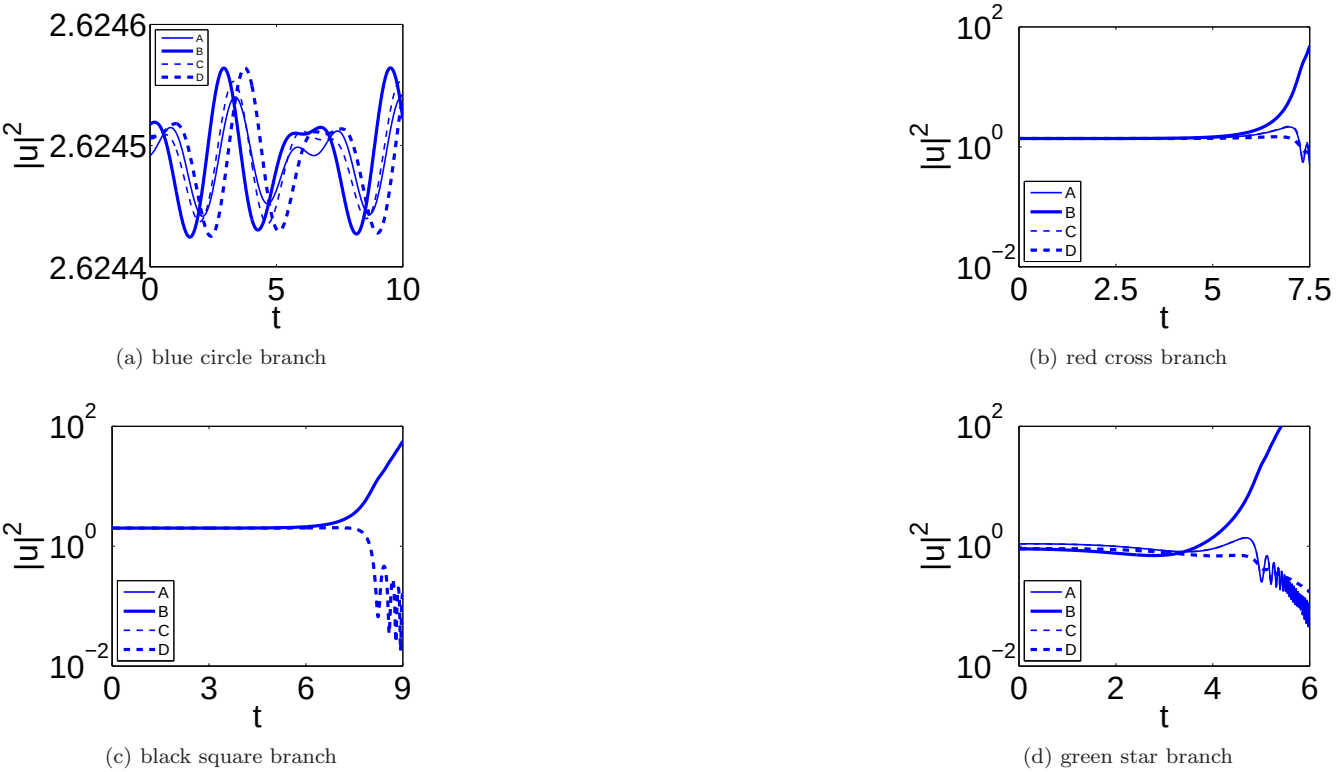

FIG. 4: (Color online) The perturbed evolution of different branches from Figs. III A and 3 at $\gamma = 1.9$. Thin solid, thick solid, thin dashed, and thick dashed curves correspond to nodes A, B, C, D in Fig. 1(a), respectively. In panel (b), the plots pertaining to sites A and C [see Fig. 1(a)] overlap. Similarly, pairs of the plots for (A,B) and (C,D) overlap in (c), and for (A,C) they overlap in (d).

B. The plaquette of the +-+- type

We now turn to the generalized (not exactly $\mathcal{PT}$-symmetric) configuration[3] featuring the alternation of the gain and loss along the plaquette in panel (b) of Fig. 1. Indeed, the absence of $\mathcal{PT}$-symmetry in this case is mirrored in the existence of imaginary eigenvalues in the linear problem of Eqs. (27), as soon as $\gamma \neq 0$. The corresponding nonlinear solutions (with $E \notin \mathbb{R}$) are not covered by the stationary solution ansatz (31). Stationary solutions (with $E \in \mathbb{R}$) solely belong to dynamical regimes below the concrete $\mathcal{PT}-$thresholds. Apart from the two $\mathcal{PT}-$symmetry violating solutions, there should exist at least two stationary solutions which we construct in analogy to [cf. Eqs. (38)] from

$$\begin{aligned} Ea &= k(b+d) + |a|^2 a - i\gamma a, \\ Eb &= k(a+c) + |b|^2 b + i\gamma b, \\ Ec &= k(b+d) + |c|^2 c - i\gamma c, \\ Ed &= k(a+c) + |d|^2 d + i\gamma d. \end{aligned} \tag{56}$$

Substituting the Madelung representation (41) and setting $A = B = C = D$ (for illustration purposes, we focus here only on this simplest case), we obtain

$$\sin(\phi_b - \phi_a) + \sin(\phi_d - \phi_a) = \sin(\phi_b - \phi_c) + \sin(\phi_d - \phi_c) = \frac{\gamma}{k}, \tag{57}$$

$$\cos(\phi_b - \phi_a) + \cos(\phi_d - \phi_a) = \cos(\phi_b - \phi_c) + \cos(\phi_d - \phi_c) = \frac{E - A^2}{k}. \tag{58}$$

[3]) For the terminology concerning exact $\mathcal{PT}-$symmetry, spontaneously broken $\mathcal{PT}-$symmetry and completely broken $\mathcal{PT}-$symmetry see the discussion of Eqs. (15) and (16).

Further, fixing $\phi_a = \phi_c = 0$, Eqs. (57) and (58) yield

$$\sin\phi_b = \sin\phi_d = \frac{\gamma}{2k},\ A^2 = E \pm \sqrt{4k^2 - \gamma^2}. \tag{59}$$

Obviously, the solution terminates at point $\gamma = \pm 2k$. Similar to what was done above, the continuation of this branch and typical examples of its linear stability are shown in Figs. 5 and III B, respectively. From here it is seen that the blue-circle branch, which has a complex quartet of eigenvalues, is always unstable. In fact, the gain-loss alternating configuration is generally found to be more prone to the instability. The red-cross branch is also unstable via a similar complex quartet of eigenvalues. This quartet, however, breaks into two real pairs for $\gamma \geq 1.5$, and, eventually, the additional imaginary eigenvalue pair becomes real too at $\gamma > 1.74$, making the solution highly unstable with three real eigenvalue pairs. The manifestation of the instability is shown in Fig. 7, typically amounting to the growth of the amplitudes at one or more gain-carrying sites.

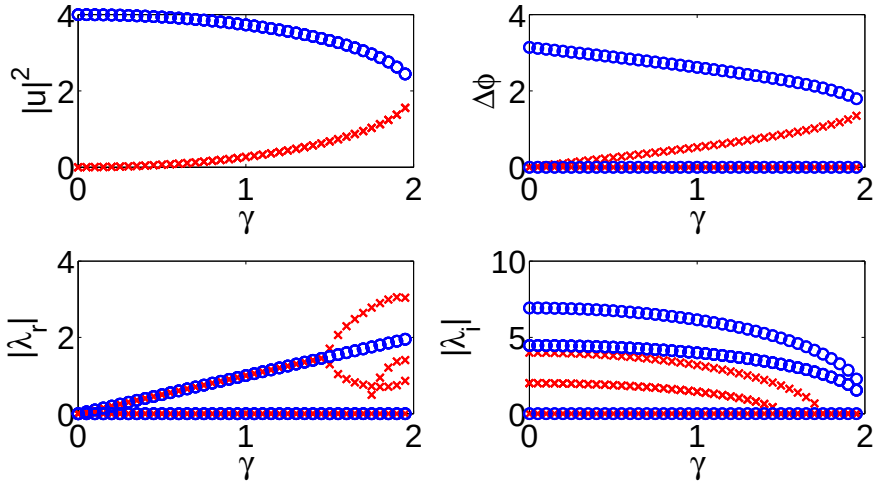

FIG. 5: (Color online) The continuation of mode (59) and its stability, supported by plaquette (b) in Fig. 1, for $E = 2$ and $k = 1$.

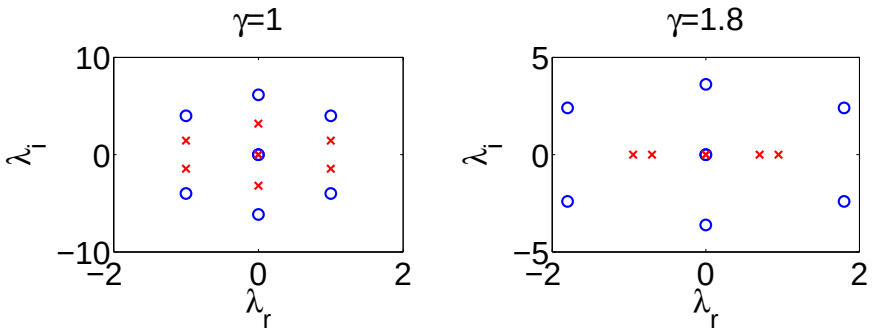

FIG. 6: Two typical stability plots for branch (59), for $E = 2$, $k = 1$ and $\gamma = 1$ and 1.8, respectively.

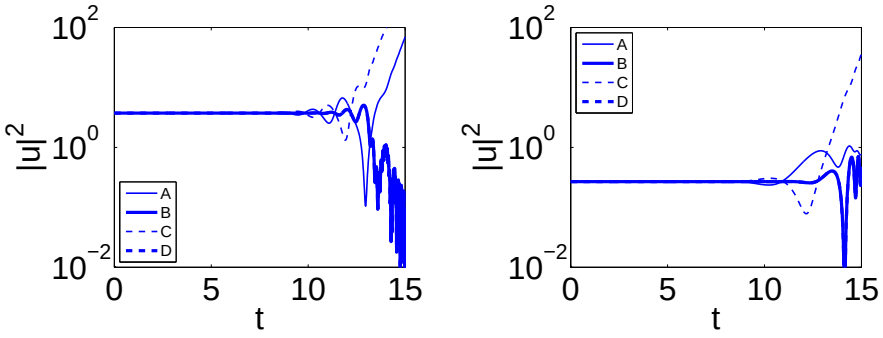

(a) blue circles branch (b) red crosses branch

FIG. 7: The perturbed evolution of the modes of type (59) at $\gamma = 1$ corresponding to the left panel of Fig. III B. The plots pertaining to sites B and D [see Fig. 1(b)] overlap in both panels.

C. The plaquette of the ++- - type

We now turn to the plaquette in Fig. 1(c), which involves parallel rows of gain and loss. In this case, the stationary equations are

$$\begin{aligned} Ea &= k(b+d) + |a|^2 a - i\gamma a, \\ Eb &= k(a+c) + |b|^2 b - i\gamma b, \\ Ec &= k(b+d) + |c|^2 c + i\gamma c, \\ Ed &= k(a+c) + |d|^2 d + i\gamma d. \end{aligned} \tag{60}$$

In this case too, we focus on symmetric states of the form of $A = B = C = D$ [see Eq. (41)], which gives rise to two solutions displayed in Fig. III C, represented by the following analytical solutions:

$$A^2 = E - k \pm \sqrt{k^2 - \gamma^2}, \tag{61}$$

$$\phi_a = \phi_b = 0, \ \sin\phi_c = \sin\phi_d = \frac{\gamma}{k}; \tag{62}$$

$$A^2 = E + k \pm \sqrt{k^2 - \gamma^2}, \tag{63}$$

$$\phi_a = 0, \ \phi_b = \pi, \ \phi_c = \phi_d - \pi, \ \sin\phi_d = \frac{\gamma}{k}, \tag{64}$$

The analysis demonstrates that the branch with the upper sign in Eq. (61) is always unstable (through two real pairs of eigenvalues), as shown by blue circles in Fig. III C. On the other hand, the branch denoted by the red crosses, which corresponds to the lower sign in Eq. (61) is stable up to $\gamma = 0.86$, and then it gets unstable through a real eigenvalue pair. The black-squares branch with the upper sign in Eq. (63) is always stable, while the green-star branch with the lower sign in Eq. (63) is always unstable. At the linear-$\mathcal{PT}$-symmetry breaking point $\gamma = k$, we observe a strong degeneracy, since all the three pairs of eigenvalues for two of the branches (in the case of the blue circles, two real and one imaginary, and in the case of red crosses— one real and two imaginary) collapse at the origin of the spectral plane. On the other hand, the black-squares branch is always stable with three imaginary eigenvalue pairs, while the green-star branch has two imaginary and one real pair of eigenvalues. Between the latter two, there is again a collision of a pair at the origin at the critical condition, $\gamma = k$. Direct simulations, presented for $\gamma = 0.5$ in Fig. 9, demonstrate the stability of the lower-sign black-squares branch, while the instability of the waveform associated with the blue circles and the green stars leads to the growth and decay of the amplitudes at the sites carrying, respectively, the gain and loss. Notice that at the parameter values considered here, the red-cross branch is also dynamically stable as shown in the top right panel of Fig. 9.

D. The plaquette of the +-0+- type

Lastly, motivated by the existence of known "cross"-shaped discrete-vortex modes in 2D conservative lattices, in addition to the fundamental discrete solitons [28, 29], we have also examined the five-site configuration, in which the

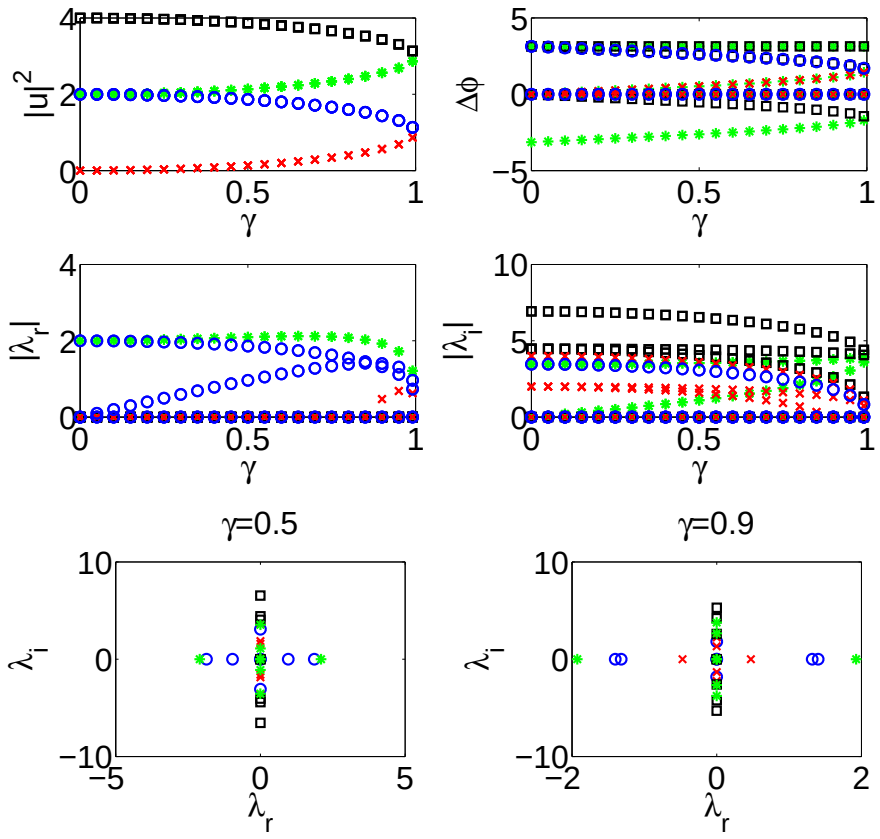

FIG. 8: (Color online) The characteristics of the mode of the ++- - type, supported by plaquette (c) in Fig. 1, and given in analytical form by Eqs. (61)- (64), for $E = 2$ and $k = 1$. The blue circles correspond to the completely unstable branch with the upper sign in Eq. (61), while the red crosses pertain to branch with the lower sign, which is stable at $\gamma < 0.86$. The black-square and green-star branches correspond to the upper and lower sign in Eq. (63), respectively. The former one is always stable, while the later one is always unstable. All four branches terminate at the critical point $|\gamma| = |k|$ of the linear $\mathcal{PT}$-symmetric system.

central site does not carry any gain or loss, while the other four feature a $\mathcal{PT}$-balanced distribution of the gain and loss, as shown in panel (d) of Fig. 1. Seeking for stationary states with propagation constant, G [instead of E in Eq. (31), as in this case we reserve label E for one of the sites of the 5-site plaquette in Fig. 1(d)], we get:

$$\begin{aligned} Ga &= kc + |a|^2 a + i\gamma a, \\ Gb &= kc + |b|^2 b - i\gamma b, \\ Gc &= k(a + b + d + e) + |c|^2 c, \\ Gd &= kc + |d|^2 d + i\gamma d, \\ Ge &= kc + |e|^2 e - i\gamma e. \end{aligned} \tag{65}$$

Similarly as before, we use the Madelung decomposition $a = Ae^{i\phi_a}, b = Be^{i\phi_b}, c = Ce^{i\phi_c}, d = De^{i\phi_d}, e = Ed^{i\phi_e}$, cf. Eq. (41), and focus on the simplest symmetric solutions with $A = B = D = E$. Without the loss of generality, we set $\phi_c = 0$, reducing the equations to

$$\begin{aligned} C^2(G - C^2) &= 4A^2(G - A^2), \\ (kC)^2 &= (\gamma A)^2 + (GA - A^3)^2, \\ \sin\phi_a &= \frac{\gamma A}{kC}, \\ \phi_a = -\phi_b &= \phi_d = -\phi_e. \end{aligned} \tag{66}$$

We report here numerical results for parameters $G = 15$, $k = 1$ (smaller G yields similar results but with fewer

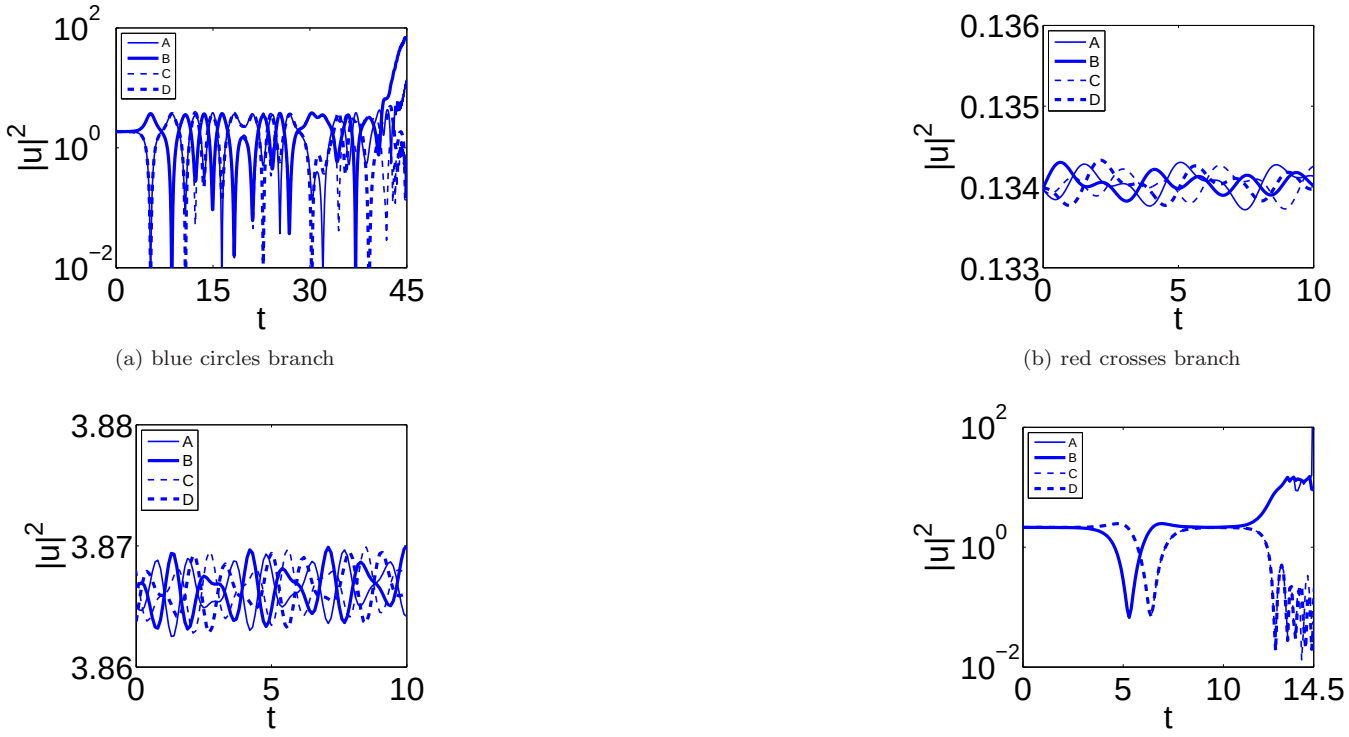

(a) blue circles branch

(b) red crosses branch

(c) black squares branch

(d) green stars branch

FIG. 9: (Color online) The perturbed evolution of the four branches of the analytical solutions given by Eqs. (61)-(64), which correspond to Fig. III C with $\gamma = 0.5$.

solution branches). We have identified five different solutions in this case, see Figs. III D and III D for the representation of the continuation of the different branches, and for typical examples of their stability (the latter is shown for $\gamma = 0.1$, 0.5 and 0.95). There are two branches (green stars and black squares) that only exist at $\gamma < 0.13$, colliding and terminating at that point. One of them has three real eigenvalue pairs and one imaginary pair, while the other branch has two real and two imaginary pairs. Two real pairs and one imaginary pair of green stars collide with two real pairs and one imaginary pair of black squares, respectively, while the final pairs of the two branches (one imaginary for the green stars and one real for the black squares) collide at the origin of the spectral plane. These collisions take place at $\gamma = 0.13$, accounting for the saddle-center bifurcation at the point where those two branches terminate. On the other hand, there exist two more branches (red crosses and magenta diamonds in Fig. III D), which collide at $|\gamma| = |k|$. One of these branches (the less unstable one, represented by magenta diamonds) bears only an instability induced by an eigenvalue quartet, while the highly unstable branch depicted by the red crosses has four real pairs (two of which collide on the real axis and become complex at $\gamma > 0.92$). Last but not least, the blue circles branch does not terminate at $\gamma = \pm k$, but continues to larger values of the gain-loss parameter, $|\gamma| > |k|$. It is also unstable (as the one represented by the magenta diamonds) due to a complex quartet of eigenvalues.

The dynamics of the solutions belonging to these branches is shown in Fig. 12. For the branches depicted by black squares and green stars (recall that they disappear through the collision and the first saddle-center bifurcation at $\gamma = 0.13$), the perturbed evolution is fairly simple: the amplitudes grow at the gain-carrying sites and decay at the lossy ones, while the central passive site (C) stays almost at zero amplitude. For the other branches, the amplitudes also grow at the two gain-carrying sites and decay at the lossy elements, while the passive site may be drawn to either the growth or decay.

IV. CONCLUSIONS AND FUTURE CHALLENGES

In the present work, we have proposed generalizations of the one-dimensional $\mathcal{PT}$-symmetric nonlinear oligomers into two-dimensional plaquettes, which may be subsequently used as fundamental building blocks for the construction of $\mathcal{PT}$-symmetric two-dimensional lattices. In this context, we have introduced four basic types of plaquettes, three

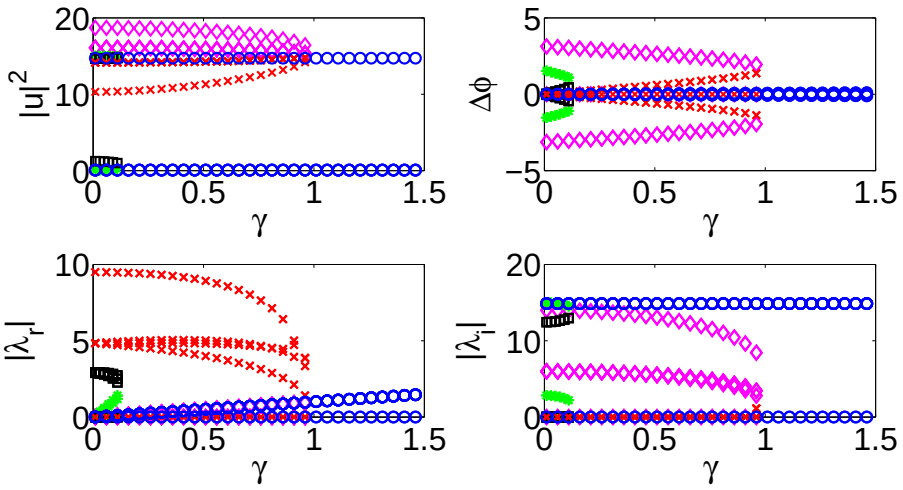

FIG. 10: (Color online) The characteristics of the different branches of solutions in the case of the five-site plaquette (d) in Fig. 1 are shown for $G = 15$ and $k = 1$. The branches represented by the chains of black squares and green stars terminate at $\gamma = 0.13$. The branches depicted by red crosses and magenta diamonds terminate at $\gamma = 1$ [i.e., at the exceptional point $|\gamma| = |k|$], while the branch formed by blue circles continues past that point.

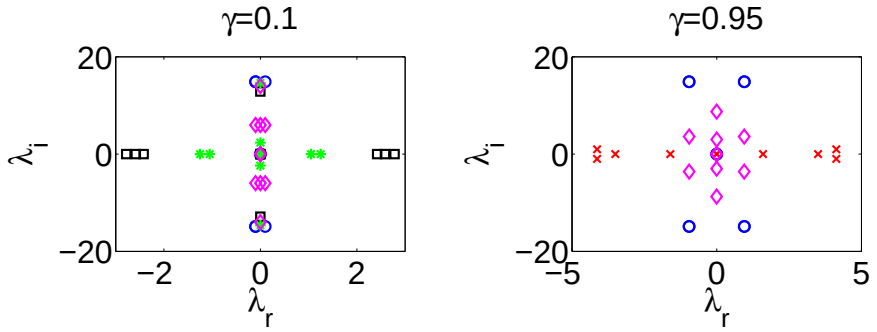

FIG. 11: (Color online) Case examples of the spectral planes of the linear-stability eigenvalues for the different solution branches shown in the previous figure, for $G = 15$, $k = 1$, and $\gamma = 0.1$ and 0.95 (from left to right).

of which in the form of four-site squares. The final one was in the form of the five-site cross, motivated by earlier works on cross-shaped (alias rhombic or site-centered) vortex solitons in the discrete nonlinear Schrödinger equation. Our analysis was restricted to modes which could be found in the analytical form, while their stability against small perturbations was analyzed by means of numerical methods. Even within the framework of this restriction, many effects have been found, starting from the existence of solution branches that terminate at the critical points of the respective linear $\mathcal{PT}$-symmetric systems — e.g., in the settings corresponding to plaquettes (a) and (c) in Fig. 1. The bifurcation responsible for the termination of the pair of branches may take a complex degenerate form [such as the one in the case of setting (a)]. Other branches were found too, that continue to exist, due to the nonlinearity, past the critical points of the underlying linear systems. In addition, we have identified cases [like the gain-loss alternating pattern (b) or the cross plaquette of type (d)] when the $\mathcal{PT}$ symmetry is broken immediately after the introduction of the gain-loss pattern. The spectral stability of the different configurations was examined. Most frequently, the stationary modes are unstable, although stable branches were found too [e.g., in settings (a) and (c)]. We have also studied the perturbed dynamics of the modes. The evolution of unstable ones typically leads to the growth of the amplitudes at the gain-carrying sites and decay at the lossy ones. It was interesting to observe that the passive sites, without gain or loss, might be tipped towards growth or decay, depending on the particular solution (and possibly on specific initial conditions).

The next relevant step of the analysis may be to search for more sophisticated stationary modes (that plausibly cannot be found in an analytical form), produced by the *symmetry breaking* of the simplest modes considered in this work, cf. Ref. [22]. The difference of such modes from the $\mathcal{PT}$-symmetric ones considered in the present work is

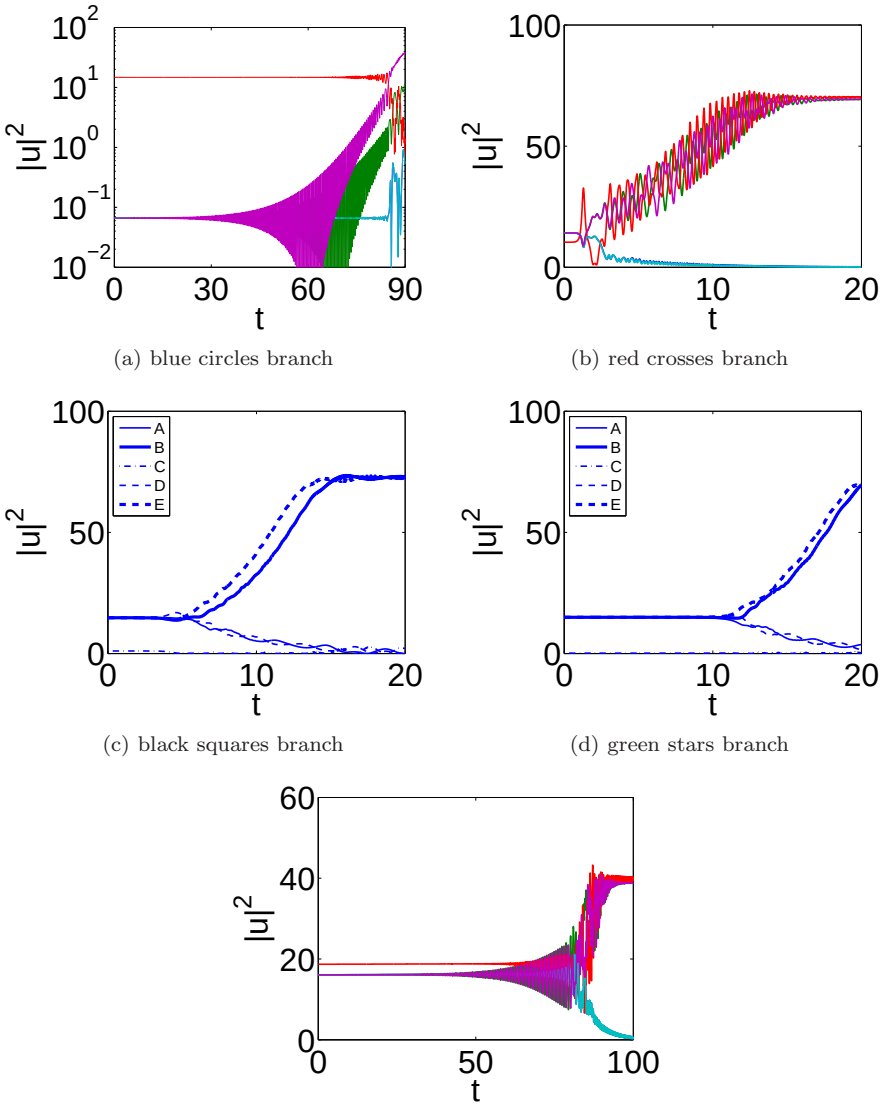

(a) blue circles branch

(b) red crosses branch

(c) black squares branch

(d) green stars branch

(e) magenta diamonds branch

FIG. 12: (Color online) The perturbed evolution for solutions belonging to different branches from Figs. III D and Fig. III D, at $\gamma = 0.1$. In panel (a), the amplitudes at the different sites of plaquette (d) from Fig. 1 (A,B,C,D,E) are depicted as follows. A: the line around 10^{-1}; B: the right one of the two triangle-like (oscillating) curves; C: the line around 10^{1}; D: overlapped by A; E: the left one of the two triangle like curves. In panel (b), the amplitudes at sites A and D overlap with each other and correspond to the bottom curve which tends to 0, while the amplitudes at sites B, C, E eventually grow to a large value. Panels (c) and (d) represent the dynamical effect of the gain at sites B and E, and loss at sites A and D, while the curve for the amplitude at site C remains very close to zero. (e) A and D overlap with each other and correspond to the bottom curve, which tends to 0; B, C, E eventually grow to values $\simeq 40$. B and D overlap with each other and C starts a little higher than those two.

the fact that modes with the unbroken symmetry form a continuous family of solutions, with energy E depending on the solution's amplitude, see Eq. (31). This feature, which is generic to conservative nonlinear systems, is shared by $\mathcal{PT}$-symmetric ones, due to the "automatic" balance between the separated gain and loss. On the other hand, the breaking of the symmetry gives rise to the typical behavior of systems with competing, but not explicitly balanced, gain and loss, which generate a single or several *attractors*, i.e., *isolated* solutions with a single or several values of the energy, rather than a continuous family. A paradigmatic example of the difference between continuous families of solutions in conservative models and isolated attractors in their (weakly) dissipative counterparts is the transition from the continuous family of solitons in the usual NLSE to a pair of isolated soliton solutions, one of which is an attractor (and the other is an unstable solution playing the role of the separatrix between attraction basins, the stable

soliton and the stable zero solution) in the complex Ginzburg-Landau equation, produced by the addition of the cubic-quintic combination of small dissipation and gain terms to the NLSE [53]. As concerns the systems considered in the present work, in the context of the breaking of the $\mathcal{PT}$ symmetry it may also be relevant to introduce a more general nonlinearity, which includes $\mathcal{PT}$-balanced cubic gain and loss terms, in addition to their linear counterparts (cf. Refs. [23] and [22]). Nevertheless, it should also be noted that the issue of potential existence of isolated solutions versus branches of solutions in $\mathcal{PT}$-symmetric systems is already starting to be addressed in the relevant literature (including in plaquette-type configurations), as in the very recent work of [33].

Moreover, the present work may pave the way to further considerations of two-dimensional $\mathcal{PT}$-symmetric lattice systems, and even three-dimensional ones. In this context, the natural generalization is to construct periodic two-dimensional lattices of the building blocks presented here, and to identify counterparts of the modes reported here in the infinite lattices, along with new modes which may exist in that case. On the other hand, in the three-dimensional realm, the first step that needs to be completed would consist of the examination of a $\mathcal{PT}$-symmetric cube composed of eight sites, and the nonlinear modes that it can support. This, in turn, may be a preamble towards constructing full three-dimensional $\mathcal{PT}$-symmetric lattices. These topics are under present consideration and will be reported elsewhere.

Acknowledgments

UG thanks Holger Cartarius and Eva-Maria Graefe for useful discussions. PGK gratefully acknowledges support from the National Science Foundation under grant DMS-0806762 and CMMI-1000337, as well as from the Alexander von Humboldt Foundation and the Alexander S. Onassis Public Benefit Foundation. PGK and BAM also acknowledge support from the Binational Science Foundation under grant 2010239.

References

[1] C. M. Bender and S. Boettcher, Phys. Rev. Lett. **80**, 5243 (1998); C. M. Bender, S. Boettcher and P. N. Meisinger, J. Math. Phys. **40**, 2201 (1999).
[2] Z. H. Musslimani, K. G. Makris, R. El-Ganainy and D. N. Christodoulides, Phys. Rev. Lett. **100**, 030402 (2008); K. G. Makris, R. El-Ganainy, D. N. Christodoulides and Z. H. Musslimani, Phys. Rev. A **81**, 063807 (2010).
[3] S. Klaiman, U. Günther, N. Moiseyev, Phys. Rev. Lett. **101**, 080402 (2008).
[4] A. Guo, G. J. Salamo, D. Duchesne, R. Morandotti, M. Volatier-Ravat, V. Aimez, G. A. Siviloglou and D. N. Christodoulides, Phys. Rev. Lett. **103**, 093902 (2009).
[5] C. E. Rüter, K. G. Makris, R. El-Ganainy, D. N. Christodoulides, M. Segev, D. Kip, Nature Phys. **6**, 192 (2010).
[6] B. A. Malomed and H. G. Winful, Phys. Rev. E **53**, 5365 (1996); H. Sakaguchi and B. A. Malomed, Physica D **147**, 273 (2000); W. J. Firth and P. V. Paulau, Eur. Phys. J. D **59**, 13 (2010); P. V. Paulau, D. Gomila, P. Colet, N. A. Loiko, N. N. Rosanov, T. Ackemann, and W. J. Firth, Opt. Express **18**, 8859 (2010); A. Marini, D. V. Skryabin, and B. A. Malomed, *ibid.* **19**, 6616 (2011); P. V. Paulau, D. Gomila, P. Colet, B. A. Malomed, and W. J. Firth, Phys. Rev. E **84**, 036213 (2011).
[7] J. Atai and B. A. Malomed, Phys. Rev. E **54**, 4371 (1996).
[8] B. A. Malomed, Chaos **17**, 037117 (2007).
[9] J. Schindler, A. Li, M. C. Zheng, F. M. Ellis and T. Kottos, Phys. Rev. A **84**, 040101 (2011).
[10] H. Ramezani, J. Schindler, F. M. Ellis, U. Günther, and T. Kottos, arXiv:1205.1847.
[11] S. Bittner, B. Dietz, U. Günther, H. L. Harney, M. Miski-Oglu, A. Richter, and F. Schäfer, Phys. Rev. Lett. **108**, 024101 (2012).
[12] H. Cartarius and G. Wunner, arXiv:1203.1885 (to be published in the present special issue).
[13] K. Li and P. G. Kevrekidis Phys. Rev. E **83**, 066608 (2011).
[14] H. Ramezani, T. Kottos, R. El-Ganainy and D. N. Christodoulides, Phys. Rev. A **82**, 043803 (2010).
[15] A.A. Sukhorukov, Z. Xu and Yu. S. Kivshar, Phys. Rev. A **82**, 043818 (2010).
[16] M. C. Zheng, D. N. Christodoulides, R. Fleischmann and T. Kottos, Phys. Rev. A **82**, 010103(R) (2010).
[17] E. M. Graefe, H. J. Korsch and A. E. Niederle, Phys. Rev. Lett. **101**, 150408 (2008).
[18] E. M. Graefe, H. J. Korsch and A. E. Niederle, Phys. Rev. A **82**, 013629 (2010).
[19] Z. Lin, H. Ramezani, T. Eichelkraut, T. Kottos, H. Cao and D. N. Christodoulides, Phys. Rev. Lett. **106**, 213901 (2011).
[20] S. V. Dmitriev, S. V. Suchkov, A.A. Sukhorukov, and Yu. S. Kivshar, Phys. Rev. A **84**, 013833 (2011)
[21] S. V. Suchkov, B.A. Malomed, S. V. Dmitriev and Yu. S. Kivshar, Phys. Rev. E 84, 046609 (2011); S. V. Suchkov, S. V. Dmitriev, B. A. Malomed, and Y. S. Kivshar, Phys. Rev. A **85**, 033835 (2012).
[22] A. E. Miroshnichenko, B.A. Malomed, and Yu. S. Kivshar Phys. Rev. A **84**, 012123 (2011).

[23] F. Kh. Abdullaev, Y. V. Kartashov, V. V. Konotop and D. A. Zezyulin, Phys. Rev. A **83**, 041805 (2011)
[24] D. A. Zezyulin, Y. V. Kartashov, and V. V. Konotop, Europhys. Lett. **96**, 64003 (2011).
[25] Y. He, X. Zhu, D. Mihalache, J. Liu, and Z. Chen, Phys. Rev. A **85**, 013831 (2012).
[26] S. Nixon, L. Ge, and J. Yang, Phys. Rev. A **85**, 023822 (2012).
[27] F. Lederer, G. I. Stegeman, D. N. Christodoulides, G. Assanto, M. Segev, and Y. Silberberg, Phys. Rep. **463**, 1 (2008).
[28] P. G. Kevrekidis *The discrete nonlinear Schrödinger equation: Mathematical Analysis, Numerical Computations and Physical Perspectives*, Springer-Verlag (Heidelberg, 2009).
[29] B. A. Malomed and P. G. Kevrekidis Phys. Rev. E **64**, 026601 (2001).
[30] D. E. Pelinovsky, P. G. Kevrekidis, D. J. Frantzeskakis, Phys. D **212**, 1 (2005).
[31] J. W. Fleischer, G. Bartal, O. Cohen, O. Manela, M. Segev, J. Hudock, and D. N. Christodoulides Phys. Rev. Lett. **92**, 123904 (2004).
[32] D. N. Neshev, T. J. Alexander, E. A. Ostrovskaya, Yu. S. Kivshar, H. Martin, I. Makasyuk, and Z. Chen, Phys. Rev. Lett. **92**, 123903 (2004).
[33] D. A. Zezyulin and V. V. Konotop, Phys. Rev. Lett. **108**, 213906 (2012).
[34] E. M. Graefe, J. Phys. A (contribution to the present special issue).
[35] V. I. Arnold, Comm. Pure Appl. Math. **29**, 557 (1976).
[36] J. Moser, Comm. Pure Appl. Math. **29** 727 (1976).
[37] M. Golubitsky and I. Stewart, Arch. Rat. Mech. Anal. **87**, 107 (1985).
[38] C. Elphick, E. Tirapegui, M. E. Brachet, P. Coullet, and G. Iooss, Physica D **29**, 95 (1987).
[39] J. Montaldi, M. Roberts and I. Stewart, Nonlinearity **3**, 695 (1990).
[40] G. M. Chechin and V. P. Sakhnenko, Physica D **117**, 43 (1998).
[41] A. Ferrando, M. Zacarés, P. Andrees, P. Fernandez de Cordoba and J. A. Monsoriu, Optics Express **13**, 1073 (2005).
[42] M. Zacarés, M. Arevalillo-Herraez and S. Abraham, Comp. Phys. Comm. **181**, 35 (2010).
[43] E. Wigner, Group Theory and Its Application to Quantum Mechanics of Atomic Spectra, (Academic Press, 1959).
[44] V. I. Arnold, Russ. Math. Surv. **26**, # 2, 29 (1972).
[45] U. Günther and F. Stefani, Czech. J. Phys. **55**, 1099-1106 (2005); math-ph/0506021.
[46] W. D. Heiss, J. Phys. A: Math. Theor. **41**, 244010 (2008).
[47] E. M. Graefe, U. Günther, H. J. Korsch, and A. E. Niederle, J. Phys. A: Math. Theor. **41**, 255206 (2008).
[48] G. Demange and E. M. Graefe, J. Phys. A: Math. Theor. **45**, 025303 (2012).
[49] M. Znojil, Rendic. Circ. Mat. Palermo, Ser. II, Suppl. **72** (2004), 211 - 218, math-ph/0104012.
[50] G. S. Japaridze, J. Phys. A: Math. Theor. **35**, 1709-1718 (2002), quant-ph/0104077.
[51] A. Mostafazadeh, J. Math. Phys. **43**, 205-214 (2002), math-ph/0107001.
[52] C. M. Bender, D. C. Brody, and H. F. Jones, Phys. Rev. Lett. **89**, 270401 (2002), quant-ph/0208076.
[53] B. A. Malomed, Physica D **29**, 155 (1987).